ADVANCES IN ATMOSPHERIC SCIENCES, VOL. 23, NO. 3, 2006, 391–404

Effects of Heterogeneous Vegetation on the Surface Hydrological Cycle

ZHOU Suoquan*[1] (周锁铨), CHEN Jingming[2] (陈镜明), GONG Peng[3] (宫 鹏), and XUE Genyuan[1] (薛根元)

[1]*Key Laboratory of Meteorological Disaster, Nanjing University of Information Science and Technology, Nanjing* 210044

[2]*Department of Geography and Program in Planning, University of Toronto*, 100 *St. George St., Room* 5047, *Toronto, Ontario, Canada M5S 3G3*

[3]*Earth Science System Institute, Nanjing University, Nanjing* 210009

(Received 16 March 2005; revised 22 July 2005)

ABSTRACT

Using the three-layer variable infiltration capacity (VIC-3L) hydrological model and the successive interpolation approach (SIA) of climate factors, the authors studied the effect of different land cover types on the surface hydrological cycle. Daily climate data from 1992 to 2001 and remotely-sensed leaf area index (LAI) are used in the model. The model is applied to the Baohe River basin, a subbasin of the Yangtze River basin, China, with an area of 2500 km^2. The vegetation cover types in the Baohe River basin consist mostly of the mixed forest type (∼85%). Comparison of the modeled results with the observed discharge data suggests that: (1) Daily discharges over the period of 1992–2001 simulated with inputs of remotely-sensed land cover data and LAI data can generally produce observed discharge variations, and the modeled annual total discharge agrees with observations with a mean difference of 1.4%. The use of remote sensing images also makes the modeled spatial distributions of evapotranspiration physically meaningful. (2) The relative computing error (RCE) of the annual average discharge is −24.8% when the homogeneous broadleaf deciduous forestry cover is assumed for the watershed. The error is 21.8% when a homogeneous cropland cover is assumed and −14.32% when an REDC (Resource and Environment Database of China) land cover map is used. The error is reduced to 1.4% when a remotely-sensed land cover at 1000-m resolution is used.

Key words: surface heterogeneity, landcover, hydrological cycle, remote sensing

doi: 10.1007/s00376-006-0391-9

1. Introduction

Vegetation obviously influences runoff, evaporation, infiltration, and soil humidity. Different cover types can have different effects on these hydrological processes. Land cover maps are therefore critical in realistic hydrological simulations, and, as such, errors due to inaccuracies in land cover data are of concern. Furthermore, many numerical models do not take into account subgrid variations of vegetation covers. Precipitation, soil humidity, and topographic index are often assumed to be the same in a grid cell, which obviously cannot accurately, reasonably, and effectively reflect the subgrid inhomogeneity of evapotranspiration, surface runoff, or precipitation affected by vegetation (Gao et al., 2004; Xue et al., 2004). Therefore, there are always significant errors in computed surface hydrology.

In fact, different mechanisms controlling runoff, infiltration, and soil humidity may exist in a grid cell (Liang and Xie, 2001), thus producing different runoff, infiltration, and soil humidity in different parts of a grid cell. Such a sub-grid inhomogeneity of vegetation in GCM models plays an important role in calculating surface runoff and directly impacts the state of soil humidity, which in turn distinctively affects seasonal rainfall (Zhou and Chen, 1995; Zhou et al., 1997; Zhou et al, 1998; Zhou et al., 1999; Zhou et al., 2003a), thus seasonal and annual climatic state (Shukla and Mintz, 1982). Since taking no account of the spatial variability of surface land-covers/vegetation types may lead to under-/over-estimation of these surface hydrologi-

*E-mail: zhousuoquan@jsmail.com.cn

cal components and subsequent soil humidity, correct land cover data are the basis for calculating surface hydrological balance and for reasonably representing interactions between the surface and the atmosphere. (Zhou et al., 2003b; Zhou et al., 2003c).

Mahmood and Hubbard (2003) discovered that different land covers may be responsible for 36% of the difference in the annual total evapotranspiration, and these remarkably change the period of soil moisture and the resultant hydrological balance. Costa-Cabral and Burges (1994) analyzed a 50-year time series of tropical streamflow and precipitation, and found that under the same precipitation conditions, when tropical forests were replaced by farmlands, the streamflow increased by 25%, on average, and by 28% in high flow seasons, and the seasonal streamflow peak occurred one month earlier. Their further analysis suggested that land cover types changed the regional surface hydrological response, indicating the large computational errors from different land covers. Sridhar et al. (2003) selected most homogeneous/inhomogeneous land surfaces in numerical experiments, and their results suggested that relative to homogeneous land surfaces, the latent heat flux of inhomogeneous land surfaces was reduced by 12% and the sensible heat increased 22%. Liu et al. (2003) used a variation coefficient of soil moisture to represent the inhomogeneity of the spatial distribution of soil moisture, and inferred that this inhomogeneity may have produced an additional mesoscale flux term. The influence of an inhomogeneous infiltration parameter on regional hydrological and climatic simulations was found to be greater than that of precipitation heterogeneity (Zeng et al., 2003).

The representation of surface inhomogeneity in the three-layer variable infiltration capacity(VIC-3L) model helps the description of the effect of vegetation on the surface hydrological process in climate models (Xue et al., 2005), thus meeting the demand of climate models in simulating hydrological effects resulting from spatially different land covers. Therefore, the VIC-3L model provides a platform for the application of remote sensing data. The use of remote sensing techniques enables us to obtain spatial and temporal information about the land surface, and thereby address issues related to inhomogenous and changing land surfaces (Engman, 1996; Ritchie and Rango, 1996). In the past 10 years, the application of remote sensing has allowed progress in hydrological research and water resource management, and in particular, the evapotranspiration distribution calculated with the satellite remote sensing spectrum data based on energy balance is of practical importance (Bastiaanssen et al., 1998). Ayenew (2003) calculated daytime potential evapotranspiration using this method and the satellite data. However, practical applications of remote sensing to hydrology are still few, and vegetation parameters, especially vegetation structure parameters, such as LAI, which plays an important role in rainfall interception, evapotranspiration and catchment water budget, have not fully been used in hydrological process modeling except in a few cases (Wigmosta et al., 1994; Chen et al., 2005). The resolution at 1 km of MODIS vegetation data can match that of VIC-3L, and furthermore VIC-3L is able to take into account the inhomogeneous distribution of vegetation in a grid cell and to calculate the contributions of various vegetation types within a grid cell to the surface water cycle.

However, the effect of varying vegetation types on surface hydrological balance is unknown, i.e., it is unknown how large an error can be caused by the variation in vegetation types (Wang et al., 2002a and b; Liu, 1997; Zhang et al., 1996; Hansen et al., 1983). In this paper, the Baohe River basin, a tributary of the Yangtze River is first selected, and then the streamflow at a hydrological station under the conditions of homogeneous and inhomogeneous vegetation distributions is simulated using VIC-3L with input of the time-varying MODIS LAI (leaf area index) data. The simulated streamflow is compared with the observations to determine the effect of inhomogeneous vegetation.

2. Brief description of the VIC-3L model

Distinctively different from general soil-vegetation-atmosphere transfer schemes (Liang et al., 1994; Nijssen et al., 1997), such as Biosphere-Atmosphere Transfer Scheme (BATS) (Dickinson et al., 1993). SiB (Sellers et al., 1986), and other distributed hydrological models, VIC-3L is based on spatially variable infiltration capacity and is able to describe the subgrid inhomogeneity of surface soil moisture, evaporation and runoff. Due to the controlling effect of vegetation on the energy and moisture exchange between the land surface and atmosphere, VIC-3L is designed to describe the variability of parameters of different surface vegetation types, such as LAI, minimum stomata resistance, roughness length, displacement height, etc. Evapotranspiration is the sum of vegetation transpiration and evaporation from wet canopies and bare soil evaporation, and in its estimation formula, both aerodynamic and canopy resistance are considered. Canopy interception is a function of LAI, and the intercepted rain evaporates at the potential rate, which can be adjusted according to canopy and aerodynamic resistances. The soil model considers three soil layers. The top layer gains moisture through rain infiltration and the moisture transfer from the top layer to the layer below is realized through the Brooks-Corey unsaturated hydraulic conductivity gravitational drainage. The radiation algo-

rithm is adapted from Thornton's scheme (Thornton and Running, 1999).

The surface evapotranspiration computation is improved in this paper. The vegetation ratio $C_{v,n}$ is used to represent the inhomogeneity of the spatial distribution of vegetation in a grid cell, which is of particular importance for GCM models at low resolutions, because a grid cell possibly contains several vegetation types and their ratios may be different in different grid cells. The VIC-3L model is able to compute evapotranspiration for the different respective vegetation types, thus raising the accuracy of the evapotranspiration estimate. However, when the effect of one type of vegetation on surface moisture is computed, the effect of the coverage or fraction of the vegetation is not taken into account. Plants thrive in summer with higher coverage and wilt in winter with a lower fraction. The vegetation coverage δ was calculated from the normalized difference vegetation index (I_{ndv}) based on Kenlo et al. (2003):

$$I_{ndv} = \frac{(R_{nir} - R_{red})}{(R_{nir} + R_{red})}\,, \tag{1}$$

$$\delta_n = \frac{(I_{ndv} - I_{ndv,\,min})}{(I_{ndv,\,max} - I_{ndv,\,min})}\,, \tag{2}$$

where $I_{ndv,\,max}$ and $I_{ndv,\,min}$ are the I_{ndv} values at full coverage δ_n=1 and no vegetation coverage δ_n=0, respectively, for the nth plant combining remote sensing vegetation types. The evapotranspiration, E, (runoff, Q) from an inhomogeneous vegetated land surface in a grid cell can be expressed as the sum of the canopy evaporation, $E_{c,n}$, transpiration, $E_{t,n}$, (surface runoff $Q_{d,n}$), and soil evaporation, E_{soil}, (under baseflow $Q_{b,n}$) for the various plant types of the land surface:

$$E = \sum_{n=1}^{N} C_{v,n}\delta_n(E_{c,n} + E_{t,n}) + C_{v,N+1}E_{soil}(1 - \delta_n) \tag{3}$$

$$Q = \sum_{n=1}^{N+1} C_{v,n}(Q_{d,n} + Q_{b,n})\,, \tag{4}$$

where $\sum_{n=1}^{N+1} C_{v,n} = 1$, $n = 1, 2, \ldots, N+1$, and $C_{v,N+1}$ denotes the area ratio of bare soil.

3. The study area and basic data

The Baohe River basin (Fig. 1), ranging from 33°40′N to 34°20′N and 106°40′E to 107°30′E, is located in the upper reaches of the Hanjiang River—the largest branch of the Yangtze River. The catchment, about 2500 km^2, covers the east of Fengxian County, the west of Taibai County, and the north of Liuba County in Shaanxi Province, and has its outlet at the Jiangkou hydrological station. The annual precipitation ranges from 500 m to 700 mm, and the terrain elevation varies from 1000 m to 1200 m.

The reasons for selecting the Baohe River basin as the study area are as follows. First, the basin is less influenced by anthropogenic activities, and is well covered with vegetation with fractions of 93%, 90%, and 50% in Taibai, Fengxian, and Liuba Counties, respectively. The basin is close to natural protection regions for wildlife, such as the giant salamander, giant panda, ibis, and Ziboshan natural protection regions. Second, the basin is relatively obturated, and the four branches of the Baohe River converge at the same hydrological

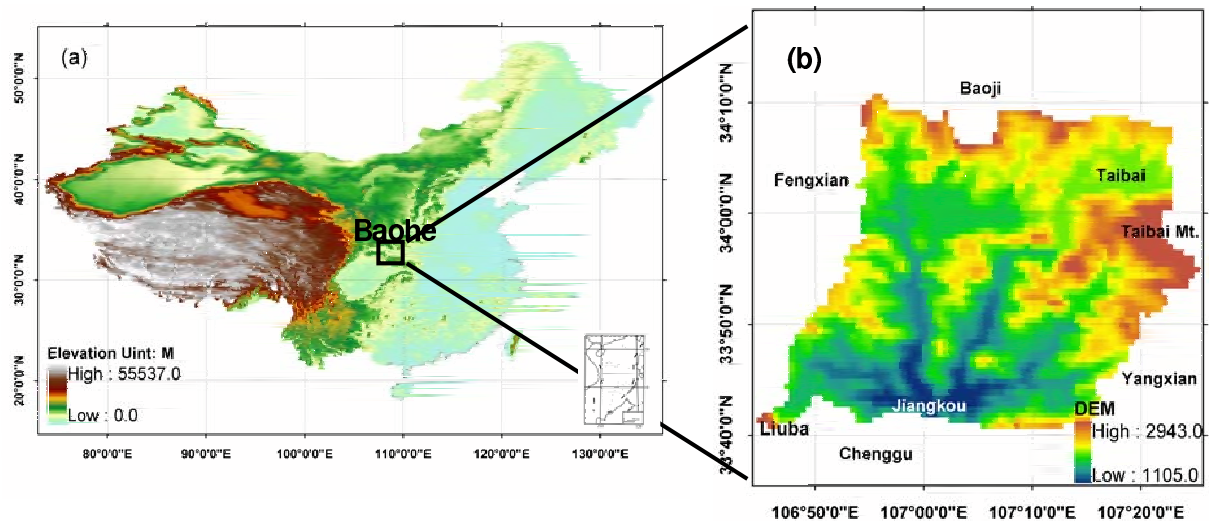

Fig. 1. (a) Location of the Baohe River basin in China, and (b) locations of the meteorological and hydrological stations in the Baohe River basin (DEM, Uints: m).

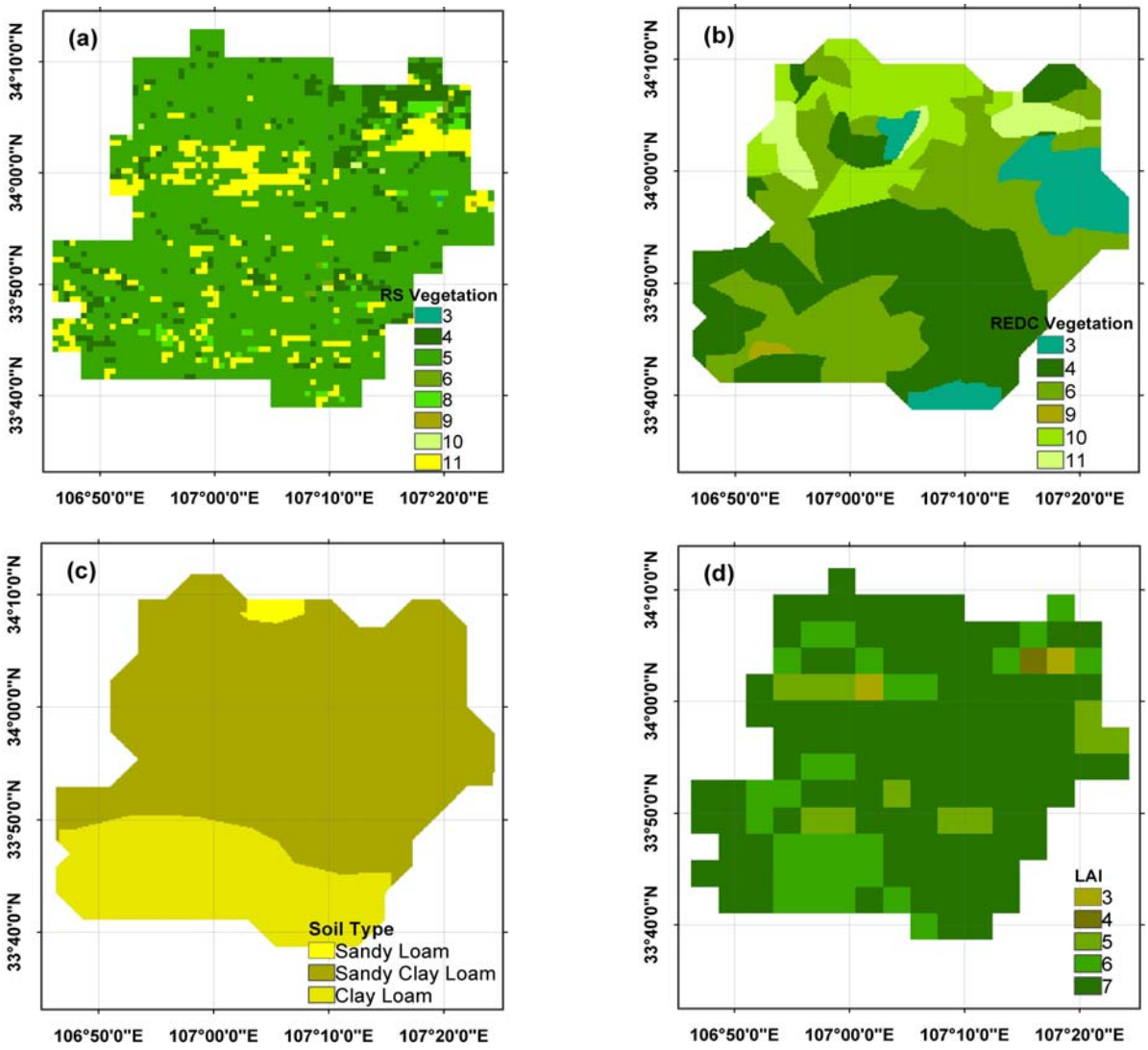

Fig. 2. (a) Vegetation types (Table 1) for the Baohe River basin based on the MODIS retrieved data in 2000 at 1-km resolution, (b) the REDC data source (see Table 1), (c) the soil types based on the REDC data source, and (d) LAI spatial distribution in June 2000 based on MODIS data resampled to 4-km resolution.

station, therefore it is relatively easy to test the water conservation of the model and to assess the effect of different vegetation distributions on hydrology. Third, the basin is the water resource area for the South-North Water Diversion (SNWD) Project in China, and the study of its surface water cycle will help the assessment of the water resources for the SNWD project, such as assessing the effect of vegetation coverage on water resources and the impact of climatic change on the SNWD, etc.

3.1 *Basic surface data*

The MODIS remote sensing products were obtained from Boston University* and the land cover was classified by a supervised International Geosphere-Biosphere Program (IGBP) classification technique. The images used were from the National Aeronautics and Space Administration (NASA) TERRA/MODIS HDF-EOS MOD12Q1. The IGBP Classification Scheme identifies 17 classes at 1-km resolution, and in combination with the land cover types of the VIC-3L model, 8 types of land covers were identified in the Baohe River basin (Fig. 2a), and correspondingly, their vegetation parameters are listed in Table 1. The existing land cover and soil type datasets for the basin, shown in Fig. 2b, were determined according to the Resource and Environment Database of China (REDC;

*ftp://crsa.bu.edu/pub/rmyneni/ myneniproducts/MODIS/MOD15_BU/C4/LAI/data/1km/2000/

Table 1. Vegetation types and their attributes.

Class	Vegetation type	Overstory	SR (s m^{-1})	MSR (s m^{-1})	June albedo	JR (m)	DH (m)
3	DNF	1	60.0	125.0	0.18	1.230	6.70
4	DBF	1	60.0	125.0	0.18	1.230	6.70
5	Mixed forest	1	60.0	125.0	0.18	1.230	6.70
6	Woody forest	1	60.0	125.0	0.18	1.230	6.70
8	Closed shrub	0	50.0	135.0	0.19	0.495	1.00
9	Open shrub	0	50.0	135.0	0.19	0.495	1.00
10	Grassland	0	25.0	120.0	0.20	0.074	0.40
11	Cropland	0	25.0	120.0	0.20	0.012	0.33

Note: DNF, deciduous needleleaf forest; DBF, deciduous broadleaf forest; SR, architecture resistance; MSR, minimum stoma resistance; JR, June roughness; DH, displacement height.

Table 2. Soil types and their attributes.

USD class	Soil type	Sand (%)	Clay (%)	Bulk density (g cm^{-3})	Field Capacity (cm^3 cm^{-3})	Wilting point (cm^3 cm^{-3})	Porosity fraction	Saturated HC (cm h^{-1})	Slope of retention curve, b
3	Sl	69.28	12.48	1.57	0.21	0.09	0.46	5.24	4.84
7	Scl	60.97	26.33	1.60	0.27	0.17	0.39	2.40	8.66
9	Cl	30.08	33.46	1.43	0.34	0.21	0.40	1.77	8.02

Note: HC, hydraulic conductivity; Sl, Sandy loam; Scl, Sandy clay loam; Cl, Clay loam.

Botanic Institute of the Chinese Academy of Sciences, 1979) and the China Land Use Map (Geographic Institute of the Chinese Academy of Sciences, 1991). The VIC-3L model identifies 12 types of soil according to the sand content. In the Baohe River basin, the soil types from the REDC source (Nanjing Soil Institute of the Chinese Academy of Sciences, 1978) include sandy loam, sandy clay loam, and clay loam (Fig. 2c), and their corresponding parameters are listed in Table 2. The LAI information is available from the MOD15A2 products, and by using the Knyazikhin algorithm (Knyazikhin et al., 1998a, b), the monthly mean LAI at 1-km resolution was aggregated into a spatial resolution of 4 km to be consistent with the spatial resolution of the other variables used in the VIC-3L model simulations. Figure 2d shows the spatial distribution of LAI in June 2000 at 4-km resolution for the Baohe River basin. The variation of LAI in one year is distinct and is associated with the crop harvest, suggesting that without these remote sensing data, it is difficult to prescribe LAI values to represent the actual circumstances.

3.2 *Model main parameters*

The VIC-3L model requires hydrological and atmospheric parameters (Table 3). The hydrological parameters include the infiltration shape parameter b_i; the distributive index of soil porosity B_p; residual moisture content Θ_r; saturated hydraulic conductivity K_{sat}; and the three base-flow-related parameters D_m, D_s, W_s, representing, respectively, the maximum subsurface flow, the fraction of D_m, and the fraction of maximum soil moisture. E_{XPT} is a parameter of the variability of K_{sat}, P_{hi_s} a soil moisture diffusion parameter, B_{ubble} the pressure of soil bubbles, D_P the soil thermal decay depth, and W_c and W_p are the critical point of soil humidity and wilting point, respectively. Table 3 provides the main parameters of each grid cell used in the routing model. Figure 3a shows the flow directions computed with ArcGIS, which are in agreement with the DEM and river networks. Figure 3b exhibits flow velocities of grid cells calculated from the terrain index (Vivek, 1999), which show a good correlation with the topographic gradient.

3.3 *Successive interpolation approach (SIA) for climatic variables*

Figure 4 shows spatial distributions of the 10-year averaged daily temperature and annual precipitation from 1992 to 2001, interpolated using the SIA (Zhou et al., 2005), which takes into account the physical process affecting the spatial variations of the meteorological variables and corrects the interpolation error step by step. Figure 4a depicts the spatial pattern of

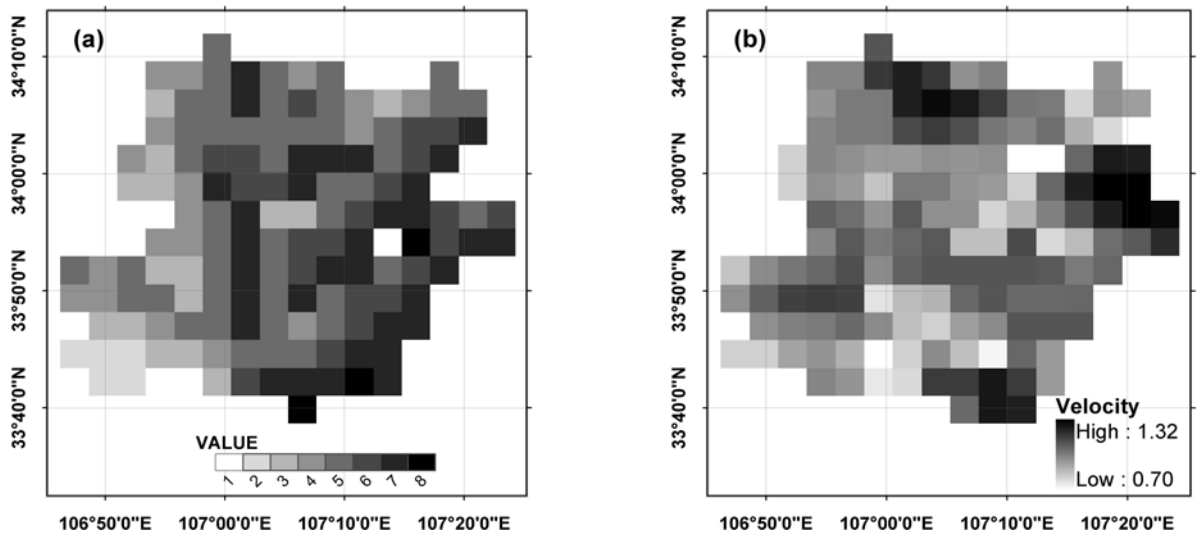

Fig. 3. The routing model parameters distribution: (a) flow directions, (b) flow velocity (units: $\mathrm{m\,s^{-1}}$).

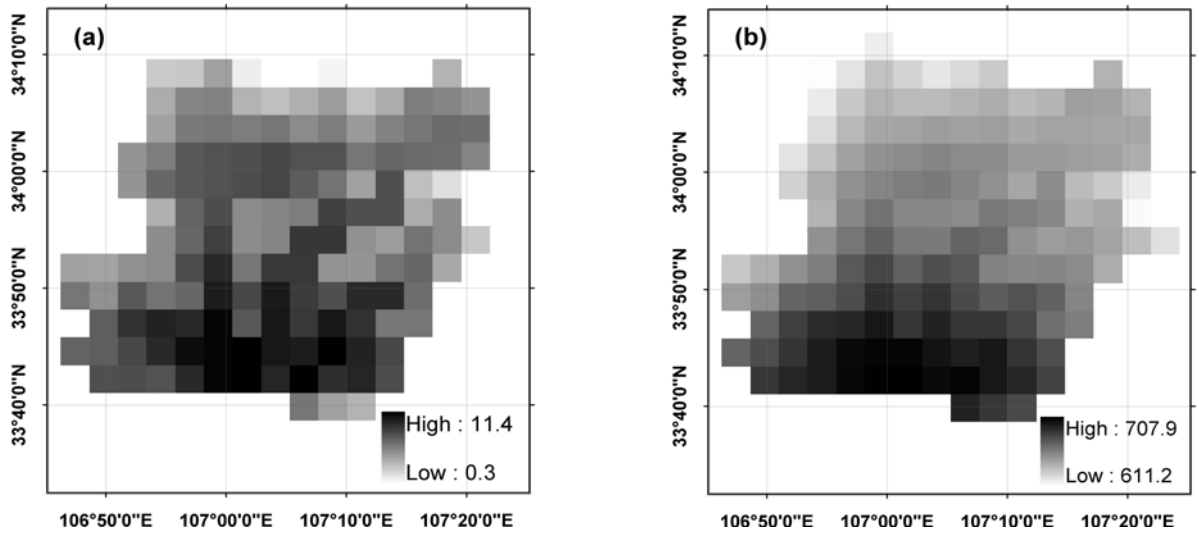

Fig. 4. Spatial distributions of the 10-year averaged climate variables (a) temperature, in °C; (b) precipitation in mm from 1992–2001, interpolated by SIA.

Table 3. VIC-3L model parameters.

Parameter	Value	Parameter	Value
b_{i}	0.03	D_{P} (m)	4.0
D_{s}	0.01	B_{ubble} (m)	0.20
D_{m}	3.0	W_{c}	0.7
W_{s}	0.65	W_{P}	0.3
E_{XPT}	10.5	P_{RCP}	623.0
K_{sat}	100.0	Θ_{r}	0.02
$P_{\mathrm{hi\_s}}$ (mm mm^{-1})	1.0	B_{P}	20.0
W_1^{c} (m)	0.20		

daily mean surface air temperature. It can be seen from Fig. 4a that the temperature obviously varies with topography. It reaches 11.4°C in the southern valley region, gradually falls northwards along the river valley, and attenuates to the minimum value of 0.3°C at peaks of the northern Taibai Mountain. The result is in good agreement with the actual observed temperatures, with the absolute errors within about 0.5–1.0°C and the relative errors less than 5%. Figure 4b illustrates the spatial pattern of the 1992–2001 averaged annual precipitation, which shows the spatial features of more (less) precipitation in the southern (northern) parts and more (less) precipitation in the mountain valley (top). However, the relationship between precipitation and terrain is not very clear. After analyzing daily precipitation distributions, we also

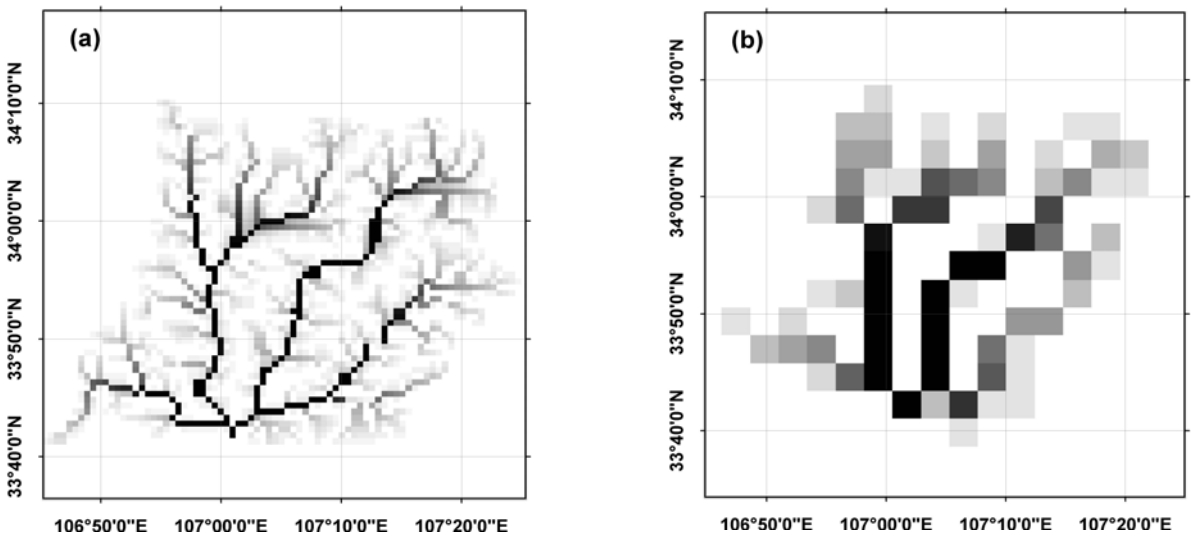

Fig. 5. Digital river networks for the Baohe River basin at two resolutions: (a) 1 km and (b) 4 km.

found that, only under certain weather conditions, does precipitation have a good relation with topography, thus statistically showing the feature that precipitation decreases with elevation. The interpolation error of the SIA for daily precipitation is 8 mm, and the relative error is less than 10%. The interpolation accuracy of the SIA is better than that of Marquínez's (Marquínez et al., 2003) multiple linear regression method.

4. The DEM and digital river network

The purpose of applying a DEM to hydrology is generally to obtain surface and subsurface flow routes, integrated river networks, and boundaries of basins (Moore et al., 1991). It is generally assumed that the flow direction in a grid cell is to one of 8 adjacent grid cells (Fairfield and Leymaire, 1991), i.e., the so-called "D8 model". Jenson's algorithm (Jenson and Domingue, 1988) assigns a flow direction for each grid cell based on the steepest slope direction (Quinn et al., 1991; Tarboton, 1994). However, the steepest slope algorithm is not correct for DEMs with a 30" (about 1 km at the equator) or even lower resolution, and larger errors will occur in the areas with less sampling points in the DEM (O'Donnel et al., 1999). Therefore, high resolution DEM information is required (Fekete et al., 2001; Olivera et al., 2002), and the flow direction is determined manually by using a simple steepest slope and lowest adjacent grid cell algorithm. Therefore this algorithm is not fully objective. Scann (2003) presented an algorithm that is able to flexibly control the flow direction on the diagonal of a grid cell and to select the generated flow direction for a coarse grid cell based on finer grid cells. Scann's algorithm was used in this paper to generate the 1-km resolution river net work and river valley boundaries (Fig. 5a), which rather accurately describe the actual water system of the Baohe River.

The study of Sridhar et al. (2003) showed that at the resolution of about 2 km it was possible to characterize the inhomogeneity of soil and vegetation. Using information at this resolution also reduces the amount of computation work. In terms of the characteristics of the large basin of the Yangtze River, the 1-km DEM was resampled to a 4-km DEM in this study, and the Baohe River network generated from the 4-km DEM is shown in Fig. 5b. Although there are much fewer details at the 4-km resolution than at the 1-km one, the major rivers and their orientations are well preserved.

5. Simulation results

5.1 *Simulation of the components of surface water balance*

Figure 6 shows the spatial distributions of the 1992–2001 climatological mean annual amounts of the surface water balance components calculated using the remotely-sensed land cover types, LAI, and soil types shown in Fig. 2. Figure 6a displays the spatial pattern of simulated evapotranspiration, where the maximum annual evapotranspiration of 606 mm occurs in the southern region, corresponding well to the maximum rainfall area. In contrast to the topography, it is also easy to find that the evapotranspiration is large in the river valley and less on the mountain top. The climate is wet (dry), and the annual rainfall large (small), in the southern (northern) part of the Baohe River basin,

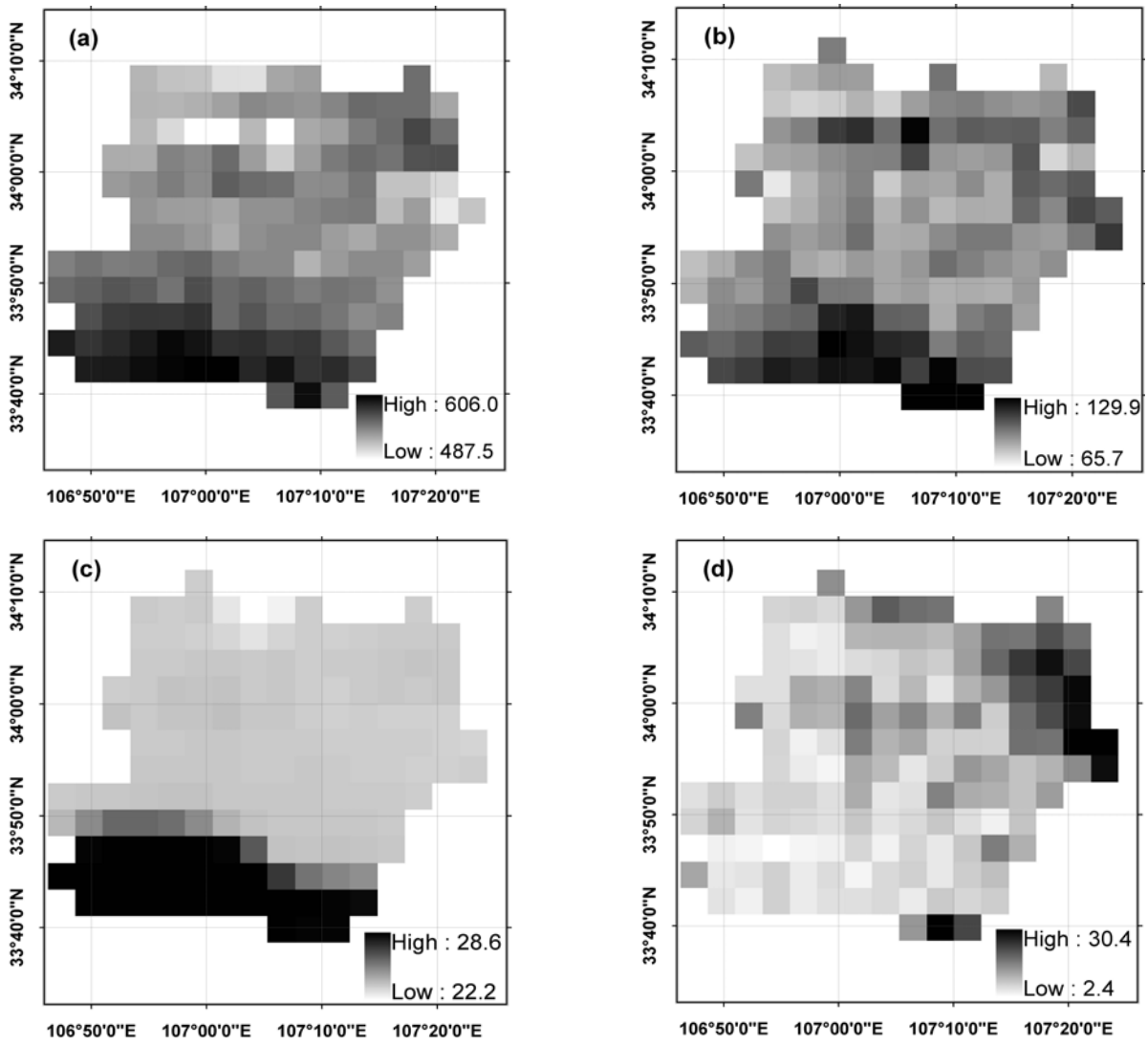

Fig. 6. Spatial distributions of the components of surface hydrological balance simulated by the VIC-3L model: (a) evapotranspiration, (b) total runoff, (c) soil moisture, and (d) snow sublimation (units: mm).

which is the major factor affecting the spatial distribution of evapotranspiration. The minimum annual evapotranspiration of 487 mm appears in the northern mountainous region, where the climate is relatively dry and cold and belongs to the semi-arid warm temperate climate. Figure 6b exhibits the spatial pattern of the simulated 10-year averaged annual runoff and substrate runoff. The runoff is large in the southern region (Fig. 6b) with low elevation where precipitation is plentiful. The area of larger runoff in the north mountainous region corresponds to one where the surface evapotranspiration is smaller, and the land cover is mainly cropland. And large runoff occurs on Taibai Mountain due to snow melting in summer. The maximum runoff of 120 mm occurs in the northeast crop area during the crop seeding and harvesting periods. Therefore, the total runoff is small in areas where the vegetation coverage is large as a result of large evapotranspiration. In the crop area, the runoff is large, and the evapotranspiration is small. Therefore the balance of the surface water over cropland is mainly determined by runoff, which suggests that cropland is susceptible to soil erosion.

Figure 6c shows the spatial distribution of the simulated climatological mean annual soil moisture in the first layer, where it can be seen that the mean moisture is spatially relatively homogeneous in the same type soil, such as being 28 mm in the southern clay loam, 23 mm in the central sand clay loam, and 22 mm in the northern sandy loam. Therefore, soil moisture is mainly affected by soil type and the spatial distribution of precipitation. However, there are still

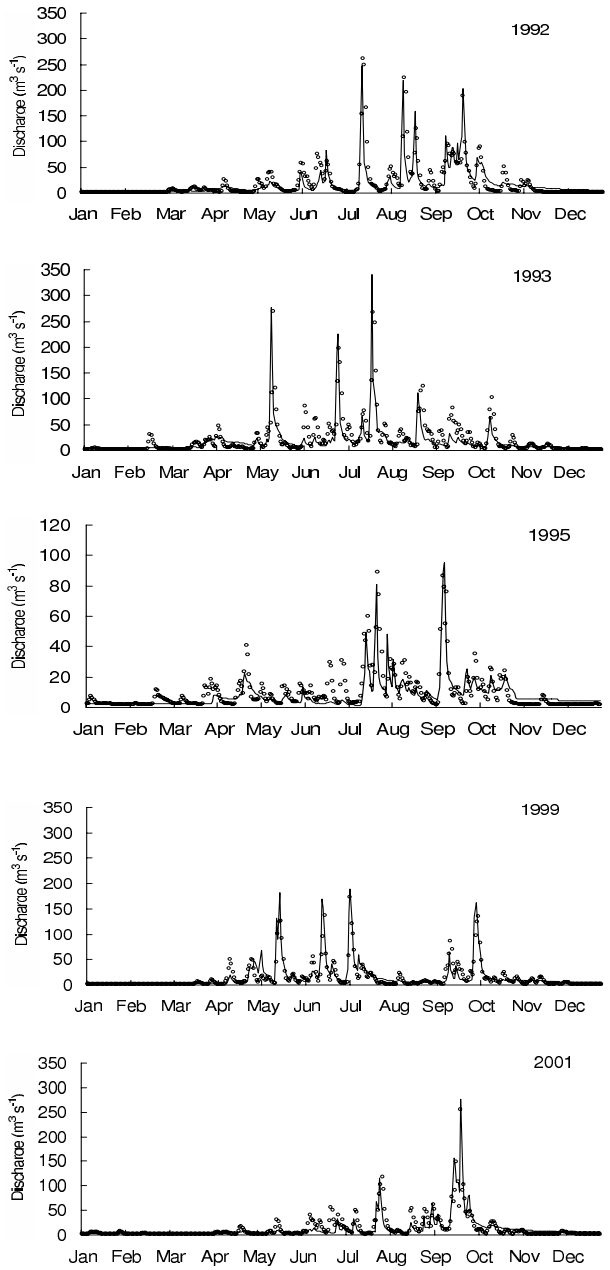

Fig. 7. Comparison of the VIC simulated discharges (units: $m^3\ s^{-1}$) at Jiangkou hydrologicalstation of the Baohe River basin and the observed ones for the 5 years in 1992–2001.

spatial differences in soil moisture even in the same soil, and these differences are related to vegetation types and slopes. Computational results show that the effect accounts for 5% of the soil moisture variance with other conditions unchanged. Figure 6c also shows that soil moisture is lowest in sandy loam with the mean annual being about 22 mm, but highest in clay loam with the annual mean being 28 mm. The porosity of sandy loam is largest in the north of the Baohe River with the semi-arid climatic zone. The soil is susceptible to the loss of moisture. Figure 6d shows the spatial distribution of simulated 10-year averaged snow sublimation. It is about 2 mm in the southern region and elevation on Taibai Mountain in the northeast region and in the northern mountainous region, exhibiting a general trend of increasing sublimation with elevation.

Based on Statistics of Hydrological Characteristics for Major Rivers in China, China Annual Runoff Depth Maps, and China Hydrological Maps, Lu and Gao (1984) calculated and plotted China Hydroclimate Maps, therein the precipitation of the Baohe River basin is about 600–700 mm, the annual evaporation about 500–600 mm, and the annual runoff about 100–150 mm. Therefore the spatial distributions of the components of surface water balance simulated using the VIC-3L model are reasonable, and the modeled evapotranspiration and surface runoff are in close agreement with those in Lu and Gao (1984).

5.2 *Discharges simulation*

After simulating the components of surface water balance using the VIC-3L model, the 10-year river discharges at the Jiangkuo hydrological station were simulated (dots in Fig. 7) using a routing model (Lohmann and Nolte-Holube, 1996) that takes into account factors such as aspect, slope, flow direction, and river network, etc. The modeled discharges were then compared with the observations (solid line in Fig. 7). The small discharges from January to April and November to December 1992 are well simulated. As the discharge increased gradually after April, small peaks occurred around June, followed by several large discharge events in July through September. All these events are closely captured by the model.

The 1993 discharge simulation better agrees with the observations than the 1992 case: three large discharges in early May, late June, and mid July are well simulated; the decreasing trends after the peaks are also well simulated; and the modeled small discharges in the winter months are consistent with observations. These results suggest that the VIC-3L model is suitable for the simulation of the surface water cycle of the Baohe River basin, although the model did not perform well in simulating two small peaks in early June and late September. The simulations in the first half of 1995 do not follow the observations closely. Discharges in late April are overestimated, and two small false fluctuations occur around June. However, after July, the model performs well in tracking the observed patterns, such as the decreasing trend from July to Au-

gust, the peak in September, and the waves of about 20 $m^3 s^{-1}$ in October.

The simulated discharges in 1999 are also in good agreement with observations. Peak values of discharges in May, June, July and October are well simulated, and the simulation errors are small. Meanwhile, the simulated small discharges in autumn, winter and spring are in accord with observations. The model is able to mimic all waves from April to October, especially the large ones. However, the model did not coincide with several small peaks. This is a problem consistently occurring in most of the years. The simulations for the summer and autumn in 2001, especially the simulated peak in late September, are also very satisfactory. However, several small waves in spring, early summer, and August are again not missed partly by the model.

It can be seen from Fig. 7 that VIC-3L is able to reconstruct the hydrological station discharge observations after using remotely-sensed vegetation types and LAI, because the remotely-sensed LAI captures well its actual seasonal variations, and the remotely-sensed land cover map contains useful information of the actual distribution of surface vegetation. Although the VIC-3L model adopts prescribed LAI with seasonal variations, we expect that the prescribed LAI may differ considerably from the reality as the tree ages may be different in the same vegetation type, and their LAI values would vary with age. The remotely-sensed LAI would capture this difference spatially, and therefore, help improve the discharge simulation.

6. Simulated results with homogeneous and inhomogeneous

6.1 *Simulation of Evapotranspiration*

Figure 8 shows the spatial distribution of the VIC-3L simulated surface evapotranspiration (ET) from four types of land covers. When the watershed is covered with homogeneous broadleaf deciduous forests (Fig. 8a), the simulated ET exhibits small spatial differences and is gradually reduced from south to north and from east to west with the maximum value of 596 mm in the southern part of the basin and the minimum value of 539 mm in the northwest, which is basically in agreement with the distribution of the annual mean rainfall and not correlated to topography. If the watershed is covered by cropland, the simulated surface evapotranspiration (Fig. 7b) fully reveals the topographic influence on evapotranspiration. It is relatively large in the river valley area and small in the mountain ridge area, suggesting that evapotranspiration on one hand is affected by the spatial distribution of precipitation, exhibiting a south-north decreasing trend. On the other hand, it is also affected by temperature, showing a valley-to-mountain decreasing trend. The maximum evapotranspiration is 598 mm in the southern valley region, and the minimum value is 461 mm on Taibai Mountain which is over 3000 m in elevation. It is seen from the comparison of Figs. 8a and 8b that evapotranspiration for broadleaf deciduous forests is generally greater than that for croplands.

When the heterogeneous REDC landcover was used in the simulation, the spatial distribution (Fig. 8c) of the simulated evapotranspiration has a good relationship with the surface vegetation types. The maximum value of 588 mm lies in the southern broadleaf deciduous forest area, not in the river valley area; the minimum value of 485 mm occurs in the northern grassland, not on the highest mountain top. Therefore, the impact of vegetation distribution on the computed surface evapotranspiration is considerable, and the spatial distribution of the evapotranspiration shows no evident relation with topography due to surface vegetation cover. The computed surface evapotranspiration using the heterogeneous remotely-sensed land cover map differs from the above three cases in spatial pattern (Fig. 8d), and sometimes there may exist an obvious difference between two adjacent grid cells. The maximum evapotranspiration reaches 606 mm in the southern region due to the influence of precipitation. The minimum value of 487 mm occurs in the northern cropland area, which is in agreement with the case shown in Fig. 8c. It is large in the thriving vegetation cover region and small in the bare soil region.

6.2 *Simulation of long-term mean hydrological station river discharge*

It can be seen from the above analyses that the surface evapotranspiration is closely related to vegetation type. The computational results also reveal that the inhomogeneity of land cover affects the surface runoff. Many previous studies have investigated the effect of the inhomogeneity and have obtained meaningful results (Lohmann and Nolte-Holube, 1996; Cai and Chen, 2003; Ma et al., 2004). However, the discharge change resulting from the inhomogeneity of land cover has not been quantitatively calculated so far, therefore, the maximum possible computational error resulting from land cover differences, which is very important for the study of the land surface process, cannot be determined. In order to assess the error caused by inhomogeneous land covers, the river discharges under different land cover types were simulated in this study, and the 10-year averaged river discharges are

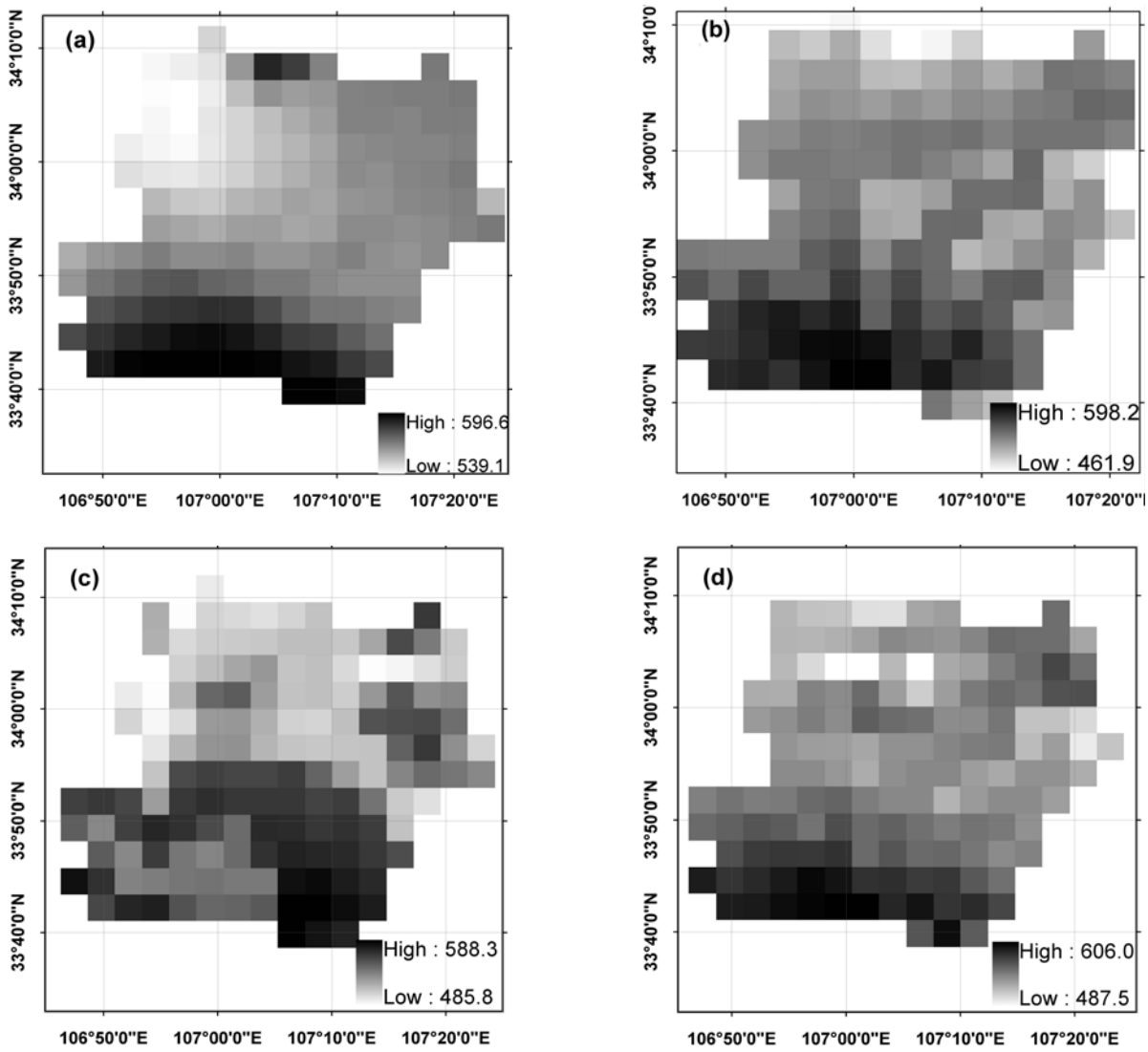

Fig. 8. Surface evapotranspiration simulated with four different vegetation types. (a) homogeneous broadleaf deciduous forest, (b) homogeneous cropland, (c) heterogeneous REDC landcover, (d) heterogeneous remote sensed landcover. (Units: mm)

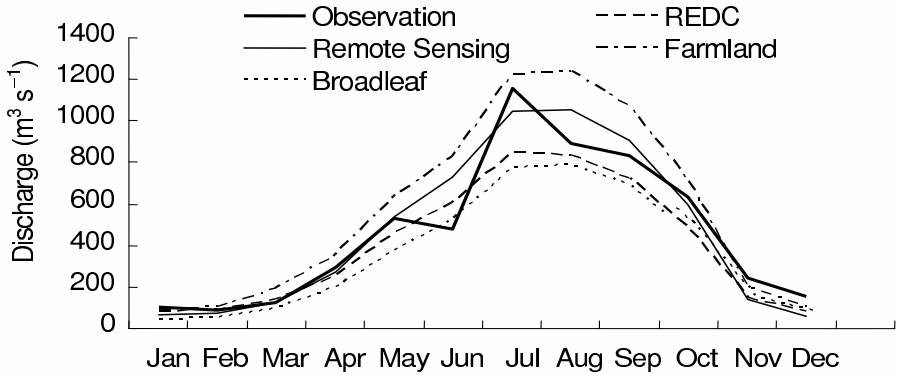

Fig. 9. Simulated annual mean discharges (units: $m^3\ s^{-1}$) at Jiangkou station for homogeneous and heterogeneous vegetation.

compared with the observed means at the Jiangkuo hydrological station.

Figure 9 shows the simulated annual mean discharges for the homogeneous and heterogeneous cases and the corresponding observations at the Jiangkuo station. The computational error is smallest in winter and largest in summer. The discharge gradually increases from winter to summer, but is rapidly reduced from summer to winter. The trends of several simulated long-term mean seasonal discharge curves are basically in accord with that of the observations, which oscillates between the simulated curves. The computed annual discharge for the case of broadleaf deciduous forest is smallest, and its annual mean error reaches −24.82%. The computed total discharge for heterogeneous REDC landcover is the next smallest, and its annual mean error is −14.32%. In these two cases, the vegetation evaporative demands are high, causing relatively small runoff, and therefore the simulated discharges are smaller than the observed. The simulated discharge for the case of homogeneous cropland is largest, and its annual mean error is +21.82%. Since crops generally have a smaller LAI than forests, the evapotranspiration from crops is smaller than the forest case, resulting in larger runoff. In comparison with the observations, the error is smallest (1.43%) in the computed discharge based on the heterogeneous remotely-sensed landcover.

7. Conclusions

The spatial distributions of surface water balance components in the Baohe River basin have been simulated in this study using MODIS land cover and LAI maps so as to take into account subgrid variations of vegetation cover in one grid cell. The simulated discharges at the Jiangkou hydrological station are compared with observations. In order to investigate the impacts of land covers on the water cycle, the surface evapotranspiration for four different land covers are simulated using the VIC-3L model. These simulated annual mean discharges are compared with each other and with observations to draw the following conclusions:

(1) The spatial distributions of simulated surface evapotranspiration, runoff, soil moisture, and underground runoff from 1992 to 2001 show that the surface evapotranspiration is mainly affected by the spatial distribution of precipitation, but in the meantime, the impacts of topography and vegetation type are also obvious. The surface evapotranspiration is relatively large in the river valley and thriving vegetation areas, and small on the mountain tops and in sparse vegetation areas. The surface runoff is influenced not only by the spatial distribution of precipitation but also by vegetation. The surface runoff is larger in sparser vegetation regions and on the perpetually snow-covered mountain tops. The soil moisture is mainly affected by the spatial pattern of precipitation, and the influence of soil type on soil moisture is about 5%. The 10-year mean value of snow sublimation indicates that the simulated value reaches its maximum on the top of the perpetually snow-covered Taibai Mountain top.

(2) Multiple-year simulated hydrological discharges are basically consistent with station observations, suggesting that the remotely-sensed land cover and LAI used provided useful information on the heterogeneous land surface for the hydrological simulations. The remotely-sensed LAI captured the seasonal variations in vegetation, and the remotely-sensed vegetation type distribution provided updated information to quantify the subgrid heterogeneity. The VIC-3L made an effective use of these remotely-sensed surface parameters to simulate the effects of multiple vegetation in one grid cell on surface evapotranspiration, runoff, etc. When remote sensing information is used, the computed spatial distributions of the surface water balance components such as evapotraspiration, evaporation, and runoff become physically meaningful.

(3) The distribution of the calculated evapotranspiration for homogeneous broadleaf deciduous forest is mainly determined by the annual mean precipitation, and not related with topography. However, in the case where the watershed is assumed to be covered by crops, the spatial patterns of evapotranspiration are not only affected by precipitation but also by topography. Overall, the evapotranspiration for broadleaf deciduous forests is greater than that for crops. The spatial distribution of the computed evapotranspiration for heterogeneous land covers is closely related to vegetation type. The vegetation transpiration is larger in vegetation with high LAI values than in sparse vegetation with low LAI values. The surface evapotranspiration is relatively large in vegetation covers with large LAI, and small in bare soil regions.

(4) The annual mean error of the computed total discharge, when compared with observations, is largest at −24.82% when the watershed is assumed to be uniformly covered with broadleaf deciduous forests. If the REDC landcover is used instead, the error is decreased to −14%. In these two cases, forests dominate the landscape, and the evaporative demands are high, causing high ET and low runoff. If the watershed is assumed to be covered by crops, the error in the discharge simulation became +21.82%. This is due to the fact that crops are generally sparse (low LAI), caus-

ing low ET and high runoff. This simulation error is reduced to 1.4% when a remotely-sensed land cover map is used, suggesting the importance of a realistic representation of the land surface conditions in the simulations of surface hydrology and land-atmosphere interaction.

Acknowledgments. This work was supported jointly by the National Natural Sciences Foundation of China (40128001/D05, 49375248) and the Science and Technology Committee of Zhejiang Province (C33, 2004C33082); State Key Laboratory of Remote Sensing Science (SK050004).

REFERENCES

Ayenew, T., 2003: Evapotranspiration estimation using thematic mapper spectral satellite data in the Ethiopian rift and adjacent highlands. *J. Hydro.*, **279**, 83–93.

Bastiaanssen, W. G. M., R. A. Menenti, and F. Holtslag, 1998: The surface energy balance algorithm for land (SEBAL), Part I Formulation. *Hydrology*, **213**, 198–298.

Botanic Institute of the Chinese Academy of Sciences, 1979: *China Vegetation Map*, China Map Press, Beijing, 512pp. (in Chinese)

Cai Xuehui, and Chen Jiayi, 2003: Geostrophical forced flows and momentum transfer in heterogeneous convective boundary layers. *Journal of Atmospheric Sciences*, **27**, 381–388. (in Chinese)

Chen, J., X. Chen, W. Ju, and X. Geng, 2005: A remote sensing-driven distributed hydrological model: Mapping evapotranspiration in a forested watershed. *J. Hydrol.,* **305**, 15–39.

Costa-Cabral, M. C., and S. J. Burges, 1994: Digital elevation model networks: A model of flow over hillslopes for computation of contributing and dispersal areas. *Water Resour. Res.,* **30**, 1681–1692.

Dickinson, R., A. Henderson-Sellers, and P. J. Kennedy, 1993: Biosphere Atmosphere Transfer Scheme (BATS) version 1E as coupled to the NCAR Community Climate Model. NCAR, Tech Note. NCAR/TN-387+STR, 72pp.

Engman, E. T., 1996: Remote sensing applications to hydrology: Future impact. *Hydrological Sciences*, **41**, 637–647.

Fekete, B. M., C. J. Vorosmarty, and R. B. Lammers, 2001: Scaling gridded river networks for macroscale hydrology: Developmet, analysis, and control of error. *Water Resour. Res.*, **37**, 1955–1967.

Fairfield, J., and P. Leymaire, 1991: Drainage networks from grid digital elevation models. *Water Resour. Res.*, **27**, 109–717.

Gao, Z., N. Chae, J. Kim, J. Hong, T. Choi, and H. Lee, 2004: Modeling of surface energy partitioning, surface temperature, and soil wetness in the Tibetan prairie using the Simple Biosphere Model 2 (SiB2). *J. Geophys. Res.*, **109**(D06102), 1–11.

Geographic Institute of the Chinese Academy of Sciences, 1991: *China Land Use Map*. Mapping, Beijing Press, 104pp. (in Chinese)

Hansen, J., G. Russell, and D. Rind, 1983: Efficient three-dimensional global model for climate studies: Models I and II. *Mon. Wea. Rev.*, **111**, 609–662.

Jenson, S. K., and J. O. Domingue, 1988: Extracting topographic structure from digital elevation data for geographic information system analysis. *Photogramm. Eng. Remote Sens.,* **54**, 1593–1600.

Kenlo, N., R. Remakrishna, N. Steven, and W. Running 2003: An operational remote sensing algorithm of land surface evaporation. *J. Geophys. Res.,* **108**(D9), 4270–4284.

Knyazikhin, Y., J. V. Martonchik, and D. J. Diner, 1998a: Estimation of vegetation canopy leaf area index and fraction of absorbed photosynthetically active radiation from atmosphere corrected MISR data. *J. Geophys. Res.*, **103**(D24), 32239–32256.

Knyazikhin, Y., J. V. Martonchik, and R. B. Myneni, 1998b: Running Synergistic algorithm for estimating vegetation canopy leaf area index and fraction of absorbed photosynthetically active radiation from MODIS and MISR data. *J. Geophys. Res.*, **103**(D24), 32257–32276.

Liang, X., D. P. Lettenmaier, and E. F. Wood, 1994: A simple hydrologically based model of land surface water and energy flues for general circulation models. *J. Geophys. Res.,* **99**(D7), 14415–14428.

Liang, X., and Z. Xie, 2001: A new surface runoff parameterization with subgrid-scale soil heterogeneity for land surface models. *Advance in Water Resources*, **24**, 1173–1193.

Liu, C., 1997: Possible influence of climate change on China water resource. *Advance in Water Sciences,* **8**, 220–225. (in Chinese)

Liu Jingmiao, Ding Yu, and Zhou Xiuji, 2003: The influence of land surface heterogeneity on parameterization of regional mean water vapor flux. *Acta Meteorologica Sinica*, **61**, 712–717. (in Chinese)

Lohmann, D., and R. A. Nolte-Holube, 1996: Large scale horizontal routing model to be coupled to land surface parameterization schemes. *Tellus*, **48A**, 708–721.

Lu, Y., and G. Gao, 1984: *China Hydro-climatic Map*. China Meteorological Press, Beijing, 15pp. (in Chinese)

Ma Yaoming, Liu Dongsheng, and Su Zhongbo, 2004: Land surface variables and vegetation variables estimated from satellite remote sensing over inhomogeneous land surface of the Northern Tibetan Plateau. *Chinese J. Atmos. Sci.*, **28**, 23–31. (in Chinese)

Mahmood, R., and K. G. Hubbard, 2003: Simulating sensitivity of soil moisture and evapotranspiration under heterogeneous soils and land uses. *Journal of Hydrology*, **280**, 72–90.

Marquínez, J., J. Lastra, and P. Garcia, 2003: Estimation models for precipitation in mountainous regions: The use of GIS and multivariate analysis. *J. Hydrol.* **270**, 1–11.

Moore, I. D., R. B. Grayson, and A. R. Ladson, 1991: Digital terrain modeling: A review of hydrological, geomorphologic, and biological applications. *Hydrol. Processes*, **5**, 3–30.

Nanjing Soil Institute of the Chinese Academy of Sciences, 1978: *China Soil Map*. China Map Press, Beijing, 214pp. (in Chinese)

Nijssen, B., D. P. Lettenmaier, and X. Liang, 1997: Streamflow simulation for continental-scale river basins. *Water Resour. Res.,* **33**, 711–724.

O'Donnel, G., B. Nijssen, and D. P. Lettenmaier, 1999: A simple algorithm for generating streamflow networks for grid-based, macroscale hydrologic models. *Hydrological Processes*, **13**, 1269–1275.

Olivera, F., M. S. Lear, and J. S. Famiglietti, 2002: Extracting low-resolution river networks from high-resolution digital elevation models. *Water Resour. Res.,* **38**, 1231–1241.

Quinn, P., K. Beven, and Chevallier P. 1991: The predication of hillslope flow paths for distributed hydrological modeling using digital terrain models. *Hydrol. Processes*, **5**, 59–79.

Ritchie, J. C., and A. Rango, 1996: Remote sensing applications to hydrology: Introduction. *Hydrological Sciences,* **41**, 429–431.

Scann, M. R., 2003: Deriving flow directions for coarse-resolution (1-4 km) grided hydrologic modeling. *Water Resour. Res.*, **39**, 1238–1256.

Sellers, P. J., Y. Mintz, Y. C. Sud, and A. Dalcher, 1986: A simple bioshpere model (SiB) for use within general circulation models. *J. Atmos. Sci.*, **43**, 505–531.

Shukla, J., and Y. Mintz, 1982: Influence of land surface evapotranspiration on the earth's climate. *Science*, **215**, 1498–1501.

Sridhar, V., L. E. Ronald, and F. Chen, 2003: Scaling effects on modeled surface energy-balance components using the NOAH-OSU land surface model. *J. Hydrol.*, **280**, 105–123.

Tarboton, D. G., 1994: A new method for the determination of flow directions and upslope areas in grid digital elevation models. *Water Resour. Res.*, **33**, 309–319.

Thornton, P. E., and S. W. Running, 1999: An improved algorithm for estimating incident daily solar radiation from measurements of temperature, humidity, and precipitation. *Agricultural and Forest Meteorology*, **93**, 211–228.

Vivek, K. A., 1999: A river flow routing scheme for general circulation models. *J. Geophys. Res.*, **104**(D12), 14347–14357.

Wang Suorong, Huang Ronghui, and Ding Yihui, 2002a: Improvements of a distributed hydrology model DHSVM and its climatological-hydrological off-line simulation experiments. *Acta Meteorologica Sinica*, **60**, 290–300. (in Chinese)

Wang Suorong, Huang Ronghui, and Ding Yihui, 2002b: Numerical simulation experiments by nesting hydrology model DHSVM with regional climate model RegCM2/China. *Acta Meteorologica Sinica*, **60**, 421–427. (in Chinese)

Wigmosta, M. S., L. W. Vail, and D. P. Lettenmaier, 1994: A distributed hydrology-vegetation model for complex terrain. *Water Resour. Res.*, **30**(6), 1665–1679.

Xue, Y., H. M. Juang, W. P. Li, S. Prince, Y. Jiao, and R. Vasic, 2004: Role of land surface processes in monsoon development: East Asia and West Africa. *J. Geophys. Res.*, **109**(D03105), 1–24.

Xue Gengyuan, Zhou Suoquan, Sun Zhaobo, Chen Hongmei, and Ji Zongwei, 2005: The Simulation and Validation of the Land Surface Water Cycle Based on Remote Sensing. *Journal of Atmospheric Sciece*, **29**(6), 911–925. (in Chinese)

Zeng Xinmin, Zhao Ming, Su Bingkai, Tang Jianping, Zheng Yiqun, Gui Qijun, and Zhou Zugang, 2003: Simulations of a hydrological model as coupled to a regional climate model. *Adv. Atmos. Sci.*, **20**, 227–236.

Zhang Jianyuan, Zhang Silong, and Song Chuanbao, 1996: Climate change and river valley runoff simulation. *Progress in Water Sciences,* **7**(suppl.), 54–59. (in Chinese)

Zhou Suoquan, Bianba Ciren, and Chen Wanlong, 1999: The numerical experiment of the effect of Jiangsu coastal development on climate. *Scientia Meteorologica Sinica*, **19**, 323–334.

Zhou Suoquan, and Chen Wanlong, 1995: The numerical experiment of the effect of the Tibetan Plateau vegetation on the East-Asian circulation. *Journal of Nanjing Institute of Meteorology*, **18**, 536–542.

Zhou Suoquan, Chen Wanlong, and Wang Geli, 1997: Experimental study on the effect of plateau vegetation on the summer climate of China: Model, precipitation, and stream fields. *Journal of Nanjing Institute of Meteorology*, **20**, 158–164.

Zhou Suoquan, Chen Wanlong, and Xu Haiming, 1998: The nest numerical experiment of the effect of the vegetation around the Tibetan Plateau on the Asian circulation. *Journal of Nanjing Institute of Meteorology*, **21**, 85–95.

Zhou Suoquan, Dai Kan, and Chen Tao, 2003a: The improvement and verification of land surface process model. *Acta Meteorologica Sinica,* **61**, 275–290.

Zhou Suoquan, Wu Xi, and Zhang Cui, 2003b: The effect and role of surface runoff in regional climate model. *New Century Meteorological Innovation and Atmospheric Science Development—Climatic System and Change.* The Climatic Committee of the Meteorological Administration of China, China Meteorological Press, Beijing, 423pp.

Zhou Suoquan, Zhang Cui, Wu Xi, 2003c: Coupling experiment of regional climate model with river flow routing model. *GIS & RS in Hydrology, Water Resources and Environment*, Vol. I, Chen Yangbo, Ed., Sun Yatsen University Press, 742pp.

Zhou, S., P. Gong, G. Xue, and J. Chen, 2005: The SIA method for the spatial analysis of precipitation resources in the upper-middle reaches of the Yangtze. *Journal of Geographical Science*, **15**(2), 223–238.